Available online at www.sciencedirect.com
ScienceDirect
Journal of Nuclear Materials 372 (2008) 367–378
journal of nuclear materials
www.elsevier.com/locate/jnucmat

Study of secondary intermetallic phase precipitation/dissolution in Zr alloys by high temperature–high sensitivity calorimetry

C. Toffolon-Masclet *, T. Guilbert, J.C. Brachet

CEA-Saclay, Nuclear Energy Division, Nuclear Materials Department, SRMA, LA2M, 91191 Gif-Sur-Yvette, France

Received 28 January 2007; accepted 18 April 2007

Abstract

It is well established that in Zr alloys, secondary precipitate phases (SPP) have a major influence on the materials properties (corrosion and mechanical behaviour). Thus, it is of great importance to know the SPP formation and dissolution temperatures and their possible metastability as a function of the alloy chemical composition, the thermal treatments and the SPP characteristics (crystallographic structure and chemical composition). The aim of the present paper is to give an overview of the studies performed recently on different alloy families, i.e., Zr–Fe–V, Zr–Fe–Mo, Zr–Nb–Fe and Zircaloy (Zr–Sn–Fe–Cr) types. High temperature–high sensitivity calorimetry (Setaram HF-DSC) has been extensively applied on these alloys. From the experimental thermograms, we have derived the SPP fraction evolution as a function of the temperature, and also the enthalpy associated with their dissolution upon heating and precipitation upon cooling. It has thus been possible to study the reversibility of the reactions involved. Depending upon the thermal diffusivities of the alloying elements, we have shown that the alloys studied can be classified into two sub-groups:

(1) alloys with fast-diffusing elements, such as Cr, Fe, V, showing reversible phase transformations upon heating and cooling;
(2) alloys with slow-diffusing elements, such as Nb or Mo, showing metastable phase transformations, that are characterised by a partial Zr-Beta decomposition and metastable SPP precipitation upon cooling.

In addition, the sensitivity of calorimetric measurements to low fractions of SPP (less than 1%) is demonstrated.

PACS: 81.05.Bx; 81.70.−q; 81.70.Pg

1. Introduction

It is now well established that in-reactor properties and irradiation behavior of zirconium alloys strongly depend upon their microstructure. Especially, the control of the second phase precipitates (SPPs) size, nature, composition and volume fraction allow to enhance corrosion resistance, hydriding properties and also to control the grain size [1,2].

Thus it is of interest to quantify systematically the SPP transformation temperatures and volume fraction.

SPP volume fractions in Zr alloys can be determined by TEM examinations but a good statistic can only be obtained by performing many examinations which are quite time consuming [3]. Synchroton facilities allow the detection of very small volume fraction of precipitates [4], but one can only have access to this facility a limited time per year.

Until now, Differential Scanning Calorimetry has been scarcely used on Zr alloys, and mainly for the determination of temperatures of the allotropic $\alpha \rightarrow \beta$ phase transformations [5,8]. In this paper, we describe how this technique can be easily applied for the determination of volume fractions and temperature existence ranges of SPPs. This methodology has been already successfully used for

* Corresponding author. Tel.: +33 16908 2139; fax: +33 16908 7130.
E-mail address: caroline.toffolon@cea.fr (C. Toffolon-Masclet).

0022-3115/$ - see front matter © 2007 Elsevier B.V. All rights reserved.
doi:10.1016/j.jnucmat.2007.04.042

the determination of β_{Nb} volume fractions in Zr–Nb alloys [6].

In this work, we have extended this approach to other Zr based alloy families such as Zr–Sn–(Fe, Cr), Zr–Sn–(Fe, V), Zr–Sn–(Mo, Fe) and Zr–Nb–Fe(Sn) in which different kind of SPPs should precipitate.

2. Previous studies

We have recently shown that high temperature–high sensitivity calorimetry (Setaram HF-DSC) can be used to determine SPPs volume fractions [6]. Indeed, this previous study concerned precipitation kinetics of the β_{Nb} phases in Zr–Nb alloys with Nb content ranging from 0.55 wt% to 2.5 wt%Nb. The alloys were thermally treated for 5 min at 1045 °C and then water quenched. The resulting initial microstructure was constituted by a Nb supersaturated α_{Zr} matrix. The alloys have then been annealed at 570 °C for different times up to 5000 h to achieve equilibrium conditions. After each annealing time, the alloys were studied by calorimetry.

Fig. 1 shows a comparison of the portions of thermograms obtained upon heating after different times of annealing treatments of a Zr–2.5 wt%Nb alloy. The β_{Nb} precipitation occurring during the annealing treatments is underlined by the endothermic peak corresponding to the $\beta_{Nb} \rightarrow \beta_{Zr}$ re-transformation upon heating. The area of this peak is increasing as a function of the annealing time. It has been demonstrated that the area of this endothermic peak was proportional to the amount of β_{Nb} phases precipitated during the annealing treatment.

Similar studies have been performed for two other Zr–Nb alloys: Zr–0.55 wt%Nb and Zr–1 wt%Nb. It was then possible to determine the precipitation kinetics of β_{Nb} as a function of the annealing time. It can be observed on Zr–0.55 wt%Nb that the β_{Nb} fraction after long term annealing at 570 °C is very low. This is consistent with the Nb solubility in the α_{Zr} matrix, which is known to be close to ~0.50% at 570 °C [7] (see Figs. 2 and 3).

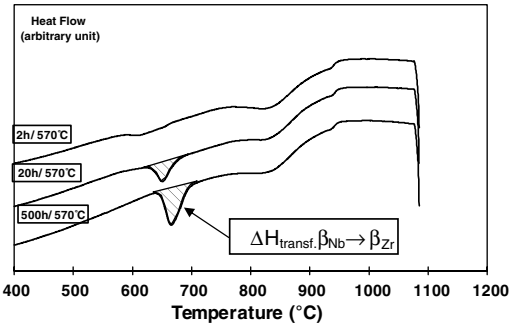

Fig. 1. Zr–2.5%Nb, initially treated at 1045 °C/5 min, water quenched and annealed at 570 °C. Comparison between thermograms obtained upon heating at 10 °C/min after 2, 20 and 500 h of annealing respectively from [6].

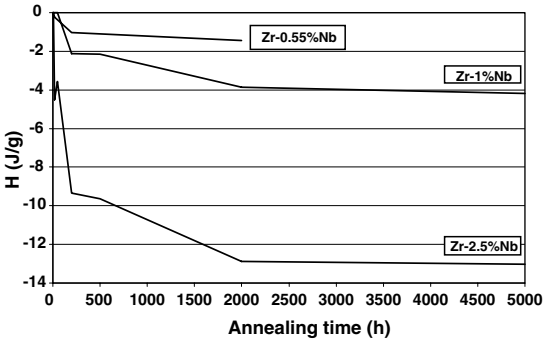

Fig. 2. Variation of the enthalpy corresponding to the on heating $\beta_{Nb} \rightarrow \beta_{Zr}$ transformation as a function of the pre-annealing time at 570 °C for 3 alloys: Zr–0.55%Nb, Zr–1%Nb and Zr–2.5%Nb from [6].

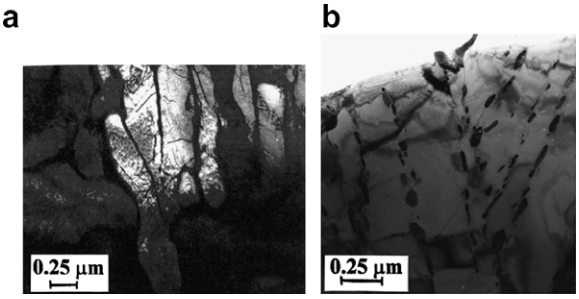

Fig. 3. TEM micrographs of a Zr–2.5%Nb initially treated at 1045 °C/5 min and water quenched (a), and a Zr–2.5%Nb initially treated at 1045 °C/5 min, water quenched, and annealed 200 h at 570 °C (b) from [6].

3. Experimental methods

3.1. Experimental materials

Part of the materials have been supplied by CEA-DRT-LTMEX. Most of them have been fabricated as small ingots by arc-melting and hot and cold rolling to produce small sheets (~1 mm thick). The other experimental materials have been supplied by AREVA-NP-CEZUS under different geometries (sheets or thick/thin tubes).

The detailed chemical compositions of the different alloys studied are reported in Table 1.

Three sets of materials can be found. The first set corresponds to pure Zr with different amounts of oxygen, the second one corresponds to Zr–Sn(Fe, Cr, V) type alloys. The third one can be divided into two subgroups: the first one corresponding to Zr–Sn–Mo–(Fe) and Zr–Nb(Fe) alloys with low iron contents ($\leqslant$1000 wt ppm Fe) and the second one corresponding to the same alloys with higher iron contents (>1000 wt ppm).

3.2. High sensitivity calorimetry

These experiments were performed using a Setaram Multi HTC high-temperature high-sensitivity calorimeter. Experiments are conducted under inert gas (pure argon

Table 1
Chemical composition of the experimental alloys studied

Alloys families	Reference	Chemical composition (wt%)							
		Sn	Fe	Cr	V	Mo	Nb	O (wt ppm)	Suppliers
Pure Zr	Zr Van Arkel	–	–	–	–	–	–	~50–100	CEA/DRT/LTMEX
	Zr (300 ppm O)	–	–	–	–	–	–	~300	AREVA-NP- CEZUS
Type Zircaloy Zr–Sn(Fe, Cr)	Zy4	1.2	**0.2**	0.1	–	–	–	1200	AREVA-NP-CEZUS
Zr–Sn(Fe, V)	Zr–1.2Sn–0.6Fe–0.3V	1.2	**0.6**	–	**0.3**	–	–	1200	CEA/DRT/LTMEX
	Zr–1.2Sn–0.3Fe–0.6V	1.2	**0.3**	–	**0.6**	–	–	1200	CEA/DRT/LTMEX
	Zr–1.2Sn–0.4V–(0.04 Fe)	1.2	<**0.02**	–	**0.5**	–	–	1200	CEA/DRT/LTMEX
Fe ⩽ 1000 ppm									
–Zr–Sn–Mo(Fe)	Zr–1.2Sn–0.5Mo–(0.03 Fe)	1.2	<**0.02**	–	–	**0.5**	–	1200	CEA/DRT/LTMEX
	Zr–0.55%Nb	–	**0.025**	–	–	–	**0.55**	1250	AREVA-NP-CEZUS
–Zr–Nb(Fe)	Zr–1%Nb	–	*0.025*	–	–	–	**1**	1250	AREVA-NP-CEZUS
	Zr–2.5%Nb	–	**0.120**	–	–	–	**2.5**	1100	Wah-Chang
Fe > 1000 ppm									
–Zr–Sn–Mo, Fe	Zr–1.2Sn–0.2Fe–0.2Mo	1.2	**0.2**	–	–	**0.2**	–	1200	CEA/DRT/LTMEX
	Zr–1.2Sn–0.6Fe–0.7Mo	1.2	**0.6**	–	–	**0.5**	–	1200	CEA/DRT/LTMEX
	Zr–1Nb–0.75Fe	<0.003	**0.75**	0.004	–	–	**1**	1300	AREVA-NP-CEZUS
	Zr–2Nb–0.45Fe	<0.003	**0.45**	0.005	–	–	**2**	1300	AREVA-NP-CEZUS
–Zr–Nb–Fe(Sn)	Zr–2Nb–0.75Fe	<0.003	**0.75**	0.005	–	–	**2**	1300	AREVA-NP-CEZUS
	Zr–1.1Nb–0.5Sn–0.4Fe	0.5	**0.4**	–	–	–	**1.1**	1350	AREVA-NP-CEZUS
	Zr–0.4Nb–0.5Fe	–	**0.45**	–	–	–	**0.4**	6000	AREVA-NP-CEZUS
	Zr–0.5Nb–0.5Fe	–	**0.45**	–	–	–	**0.5**	600	AREVA-NP-CEZUS
	Zr–0.85Nb–0.5Fe	–	**0.47**	–	–	–	**0.85**	600	AREVA-NP-CEZUS

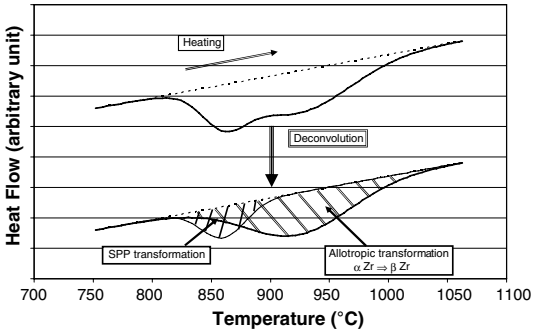

Fig. 4. Schematic representation of the deconvolution of two enthalpic peaks obtained by calorimetric measurements.

or helium) for typical heating/cooling rates ranging from 1 to 10 °C/min. The method used to determine the relative amounts of β- (or α-) phase fractions from the experimental thermograms as a function of temperature has been already presented in [8]. The same method has been extended to evaluate the relative amounts of SPPs. When the SPP and the allotropic $\alpha \leftrightarrow \beta$ phase transformations take place in the same range of temperatures, a deconvolution of the different enthalpic peaks is applied, assuming that they have both a Gaussian form, as illustrated in Fig. 4.

3.3. TEM examinations on carbon extractive replica

The SPP stoichiometries were determined using a scanning energy dispersive device (STEM/X-EDS). The carbon replica technique allows the determination of particle chemical composition without matrix contribution. This technique consists in sputtering a carbon layer on the specimen surface, followed by an electro-etching procedure in order to collect the replicas [9].

4. Experimental results

4.1. Second phase particles

Due to the very low solubility limit of Fe, Cr, Ni and V in α_{Zr} at low temperatures (⩽700 °C), different kinds of SPPs can precipitate. Thus, the phases precipitated in this case are namely: LAVES Phase type, that is $Zr(X1, X2)_2$ with an hexagonal compact ($MgZn_2$ type) and/or a cubic centered (Cu_2Mg type) crystallographic structure. We have chosen to describe the chemical compositions of the SPPs by their atomic stoichiometry $Zr(X1, X2)_2$ as presented in Table 2. One exception concerns the fcc $(Zr, Nb)_4Fe_2$ phase in the ZrNbFe system which is denoted: $(Zr, Nb)_4Fe_2$.

In Zy-4 alloys, as expected, only hexagonal $Zr(Fe,Cr)_2$ LAVES phase type SPPs are precipitated [10].

Two phases have been observed by Petkov and Svechnikov [11] in the Fe–V–Zr system: they both correspond to Laves phases. The first one is hexagonal $Zr(Fe_{1-X}V_X)_2$ corresponding to the average chemical composition $Zr_{1/3}Fe_{1/3}V_{1/3}$ and the second one is cubic $Zr(Fe_{1-X}V_X)_2$ corresponding to the average composition $Zr_{33}Fe_{17}V_{50}$ [12]. In our study, microstructural studies of Zr–1.2 wt%Sn–0.6 wt%Fe–0.3 wt%V and Zr–1.2 wt%Sn–0.3 wt%Fe–0.6 wt%V alloys show that hexagonal $Zr(Fe, V)_2$ phases are the only secondary precipitated phases in these alloys.

Table 2
Typical stoichiometries of the intermetallic phases precipitated in the different alloys

Alloys type	Zr–Sn, Fe, Cr	Zr–Sn, Fe, V	Zr–Sn–Fe, Mo	Zr–Nb, Fe, (Sn)
Intermetallic phases	$Zr(Fe,Cr)_2$	$Zr(Fe,V)_2$	$Zr(Fe,Mo)_2$ and/or $Zr_{0.6}(Fe,Mo)$	$Zr(Fe,Nb)_2$ and/or $(Zr,Nb)_4Fe_2$ and/or β_{Nb} (Nb ~ 80–90%)

Three kinds of ternary Fe–Mo–Zr phases can be found in alloys containing these elements: hexagonal $Zr(Fe_{1-x}Mo_x)_2$ with an average chemical composition $Zr_{1/3}Fe_{1/3}Mo_{1/3}$ [13], cubic $Zr(Fe_{1-x}Mo_x)_2$ with average chemical composition $Zr_{33}Fe_{63}Mo_4$ [13] and hexagonal Zr_9FeMo_4 with average composition $Zr_{64}Fe_7Mo_{29}$ [14]. In our study, two kinds of SPPs have been found in the Zr–Sn–(Fe, Mo) alloys studied, $Zr(Fe,Mo)_2$ Laves phases (hexagonal and/or cubic) and $Zr_{0.6}(Fe,Mo)$ corresponding to Zr_9FeMo_4 phase.

Two ternary intermetallic phases can be found in Zr–Nb, Fe, (Sn) alloys: a Laves phase with a hexagonal structure $Zr(Nb,Fe)_2$ (average chemical composition: $Zr_{35}Nb_{35}Fe_{30}$) and a fcc phase $(Zr,Nb)_4Fe_2$ (average chemical composition: $Zr_{60}Nb_{10}Fe_{30}$) [15–20]. Moreover, cubic centered β_{Nb} phases can be found.

4.2. Pure Zr

In this study, experiments on pure Zr were performed in order to have a reference for the experiments on Zr alloys. The endothermic and exothermic peaks on the thermograms (Fig. 5) correspond to the allotropic reaction $\alpha_{Zr} \leftrightarrow \beta_{Zr}$. It can be seen from this thermogram, that the allotropic transformation is reversible and the hysteresis between heating and cooling at 5 °C/min is very weak (~20 °C).

Two kind of alloys were studied in this part of the work: one containing ~50 wt ppm O (Van Arkel) and the other one containing around 300 wt ppm O. It can be seen from Fig. 6 that oxygen has a strong influence on the transus temperatures. These experiments point out the necessity to check oxygen contents of Zr alloys before and after performing calorimetric experiments because of potential in-situ oxidation.

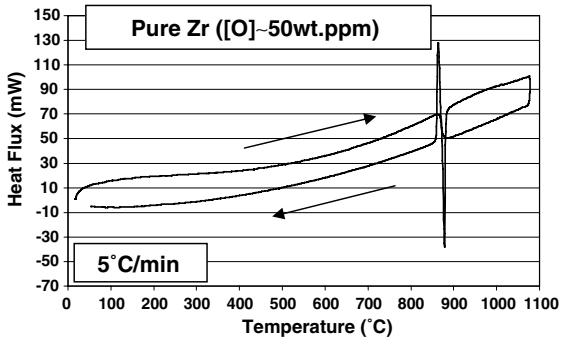

Fig. 5. Typical thermogram obtained by calorimetry for a thermal cycle (heating/cooling rate = 5 °C/min) on pure Zr (Van Arkel).

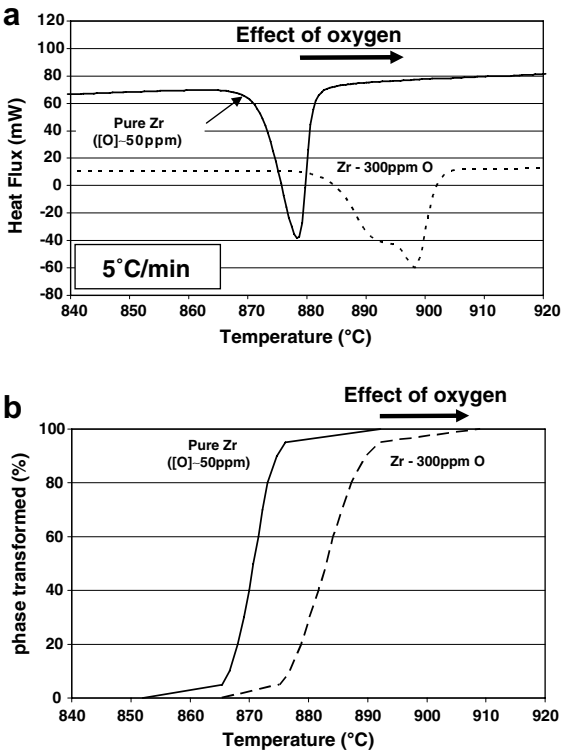

Fig. 6. Portions of thermograms (a) and βZr phase fraction deduced from calorimetric measurements (b) performed upon heating at 5 °C/min on Zr Van Arkel and Zr containing 300 ppm O.

4.3. Group 1: Zr–Sn(Fe, Cr) and Zr–Sn(Fe, V) alloys

In this group except Sn, the alloying elements, Fe, Cr and V, are fast diffusing elements and their solubility limit in the α_{Zr} solid solution is very small.

The results obtained by calorimetry for two typical alloys, that is, Zy-4 and Zr–1.2 wt%Sn–0.04 wt%Fe–0.4 wt%V, are shown below.

4.3.1. Low-tin Zy-4 (Zr–1.2 wt%Sn–0.2 wt%Fe–0.1 wt%Cr)

Fig. 7 represents a typical thermogram obtained on Zy-4 alloy (heating/cooling rate = 5 °C/min) showing two peaks both on heating and cooling. Considering their respective temperature ranges upon heating, we assume that the first endothermic peak corresponds to the $Zr(Fe,Cr)_2 \rightarrow \beta_{Zr}$ transformation, and the second one corresponds to the allotropic $\alpha_{Zr} \rightarrow \beta_{Zr}$ transformation. On cooling, the exothermic peaks correspond to the inverse reactions that is $\beta_{Zr} \rightarrow \alpha_{Zr}$ and $\beta_{Zr} \rightarrow Zr(Fe,Cr)_2$.

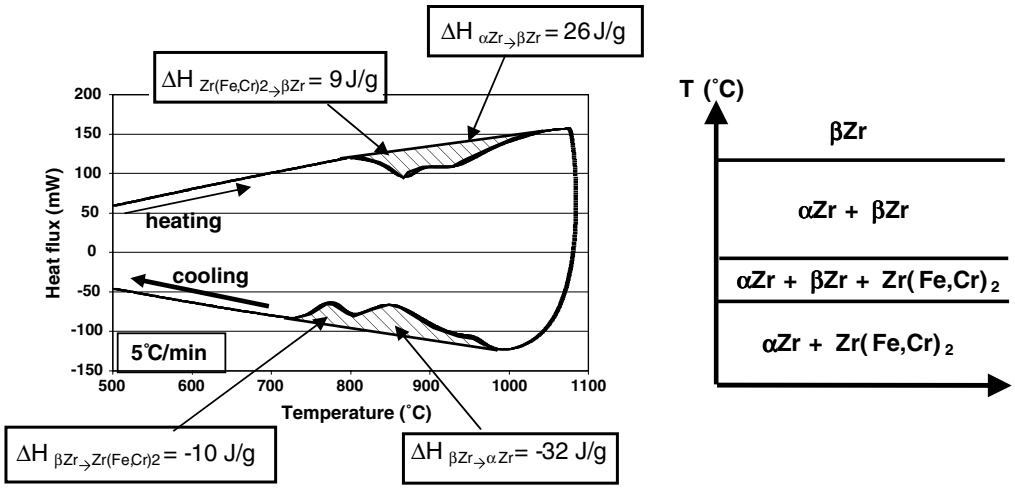

Fig. 7. Typical thermogram obtained by calorimetry on low-tin Zy-4: Zr–1.2 wt%Sn–0.2 wt%Fe–0.1 wt%Cr.

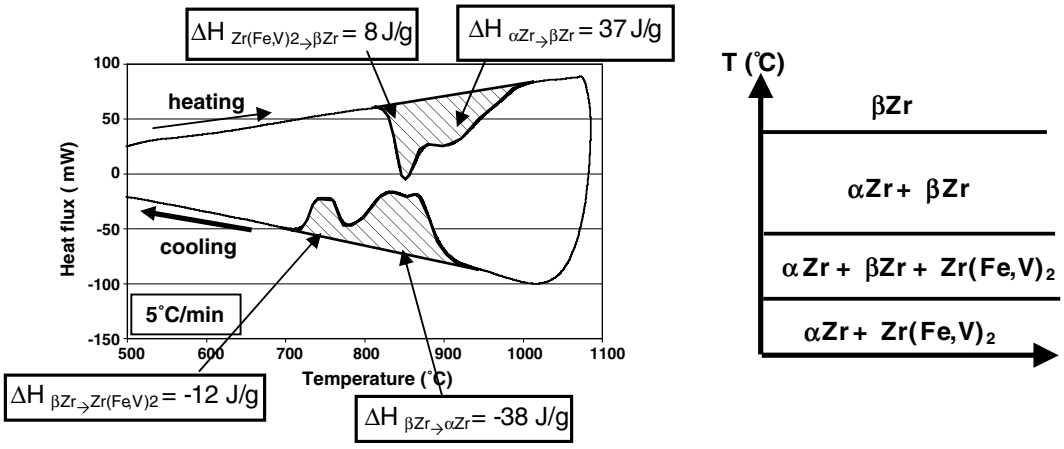

Fig. 8. Typical thermogram obtained by calorimetry on Zr–1.2 wt%Sn–0.04 wt%Fe–0.4 wt%V.

The precipitation sequence is schematically represented in Fig. 7. The reactions are reversible upon heating and cooling. The enthalpy associated to the transformation of the SPPs is very high compared to its volume fraction (less than 1 vol.%) and compared to the enthalpy associated to the full allotropic $\alpha_{Zr} \leftrightarrow \beta_{Zr}$ transformation.

4.3.2. Zr–Sn(Fe, V)

The thermogram and the associated precipitation sequence obtained for the Zr–1.2 wt%Sn–0.04 wt%Fe–0.4 wt%V alloy (Fig. 8) are very similar to the one obtained for Zy-4. The reaction upon heating and cooling is reversible. The enthalpy associated to the transformation of the SPP is very high compared to its volume fraction (~1%) and also compared to the enthalpy associated to the allotropic transformation.

4.4. Group 2: Zr–Nb–Fe(Sn) and Zr–Sn–Mo, Fe alloys

The alloys of this group are characterised by the association of fast and low diffusing alloying elements, respectively (Fe, Cr) and (Nb, Mo).

4.4.1. Fe content < 1000 ppm

4.4.1.1. Zr–Nb–Fe(Sn). For a Zr–2.5 wt%Nb–0.1 wt%Fe alloy, two[1] peaks are observed upon heating and only one upon cooling (Fig. 9). The schematic representation of the precipitation sequences associated to the thermograms clearly show that for this alloy the reaction is not reversible upon heating and cooling. On heating, a very classical precipitation sequence is observed: we assume that the first peak corresponds to the transformation $\beta_{Nb} \rightarrow \beta_{Zr}$, and the second one to the allotropic transformation: $\alpha_{Zr} \rightarrow \beta_{Zr}$.

On cooling, only one peak is observed corresponding to the reaction: $\beta_{Zr} \rightarrow \alpha_{Zr} + \beta^*_{Zr}$. Indeed, the analysis of the resulting microstructure after cooling shows that the precipitated phases inside the α_{Zr} matrix are metastable β_{Zr} enriched in Nb (~15–20 at.%) denoted: β^*_{Zr}.

[1] Because of the low Fe fraction, we did not detect the re-transformation of (Zr, Nb, Fe) ternary intermetallic compound. However, due to the very low solubility of Fe in αZr, it is likely that this reaction occurs (even for a nominal Fe content < 1000 wt ppm), but the volume fraction of SPP involved is too low to be clearly detected.

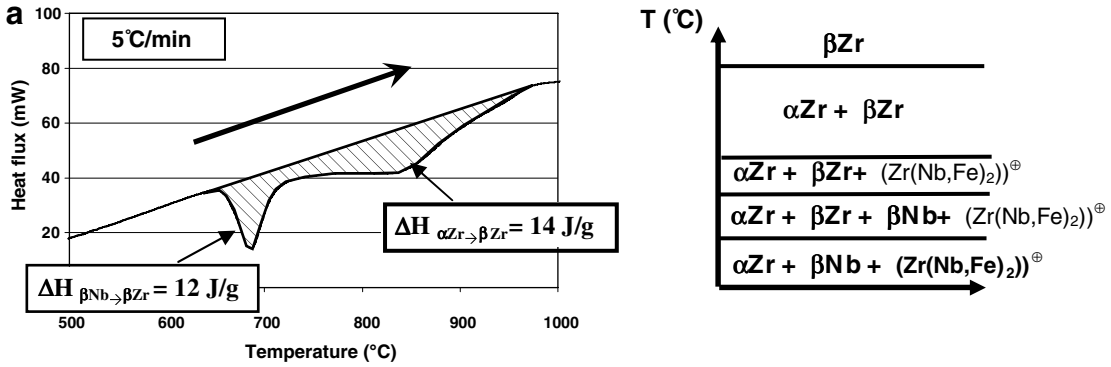

⊕ : *The $Zr(Nb,Fe)_2$ volumic fraction is too small to be detected clearly by calorimetry, but TEM examinations show that this SPP is present even for low Fe content.*

Heating

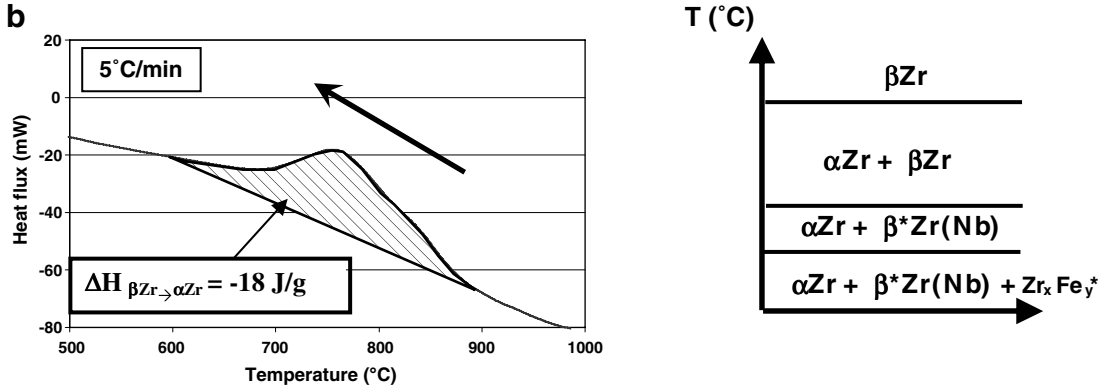

Cooling

Fig. 9. Typical thermogram obtained by calorimetry on Zr–2.5 wt%Nb–0.1 wt%Fe.

The precipitation sequences are presented in Fig. 9, showing the non-reversibility of the reaction. Upon heating, the enthalpy associated to the transformation of the SPP is very high compared to its volume fraction and also compared to the enthalpy associated with the allotropic $\alpha_{Zr} \rightarrow \beta_{Zr}$ transformation. As discussed previously [20], on cooling, Nb enriched β_{Zr} phases have not enough time to fully transforms into the $\alpha_{Zr} + \beta_{Nb}$ equilibrium phases because of the quite low ending transformation temperature (~600 °C) compared to the low diffusivity of Nb atoms. Thus, a metastable β^*_{Zr} phase, enriched with Nb (~10–15 at.%) is retained at low temperature. It is then necessary to perform quite long annealing times (>100 h) below 600 °C to decompose the β^*_{Zr} phase into $\alpha_{Zr} + \beta_{Nb}$ equilibrium phases.

4.4.1.2. Zr–Sn–Mo, Fe. A similar behaviour is observed for the alloy: Zr–1.2 wt%Sn–0.5 wt%Mo–0.03 wt%Fe. The reaction upon heating and cooling is not reversible (Fig. 10). After one thermal cycle, a metastable β^*_{Zr} enriched in Mo (~15 at.%Mo) is retained at room temperature.

4.4.2. Fe content > 1000 ppm

For the alloys containing more than 1000 wt ppm, the presence of one or two ternary Zr–Nb–Fe SPP is systematically detected by calorimetry, thanks to a higher Fe content.

4.4.2.1. Zr–Nb–Fe(Sn). For the alloy Zr–0.8 wt%Nb–0.5 wt%Fe, two or three peaks are observed on heating (see Fig. 11). We assume that the first and second ones correspond to the transformation of the SPPs and the second (or the third) one to the allotropic $\alpha_{Zr} \rightarrow \beta_{Zr}$ transformation. On cooling, two peaks are also observed, but the shape of the peak corresponding to the precipitation of the SPPs is very different from the one obtained on heating. In-situ neutron diffraction experiments [20] and TEM examinations have shown that two metastable SPPs can be retained at room temperature after the high temperature thermal cycle: a $Zr_xFe^*_y$ and a β^*_{Zr} phase (β_{Zr} enriched in Nb (~15–20 at.%Nb)).

Just as in the previous alloys studied, the enthalpies associated to the transformation of the SPPs are very high compared to their volume fractions.

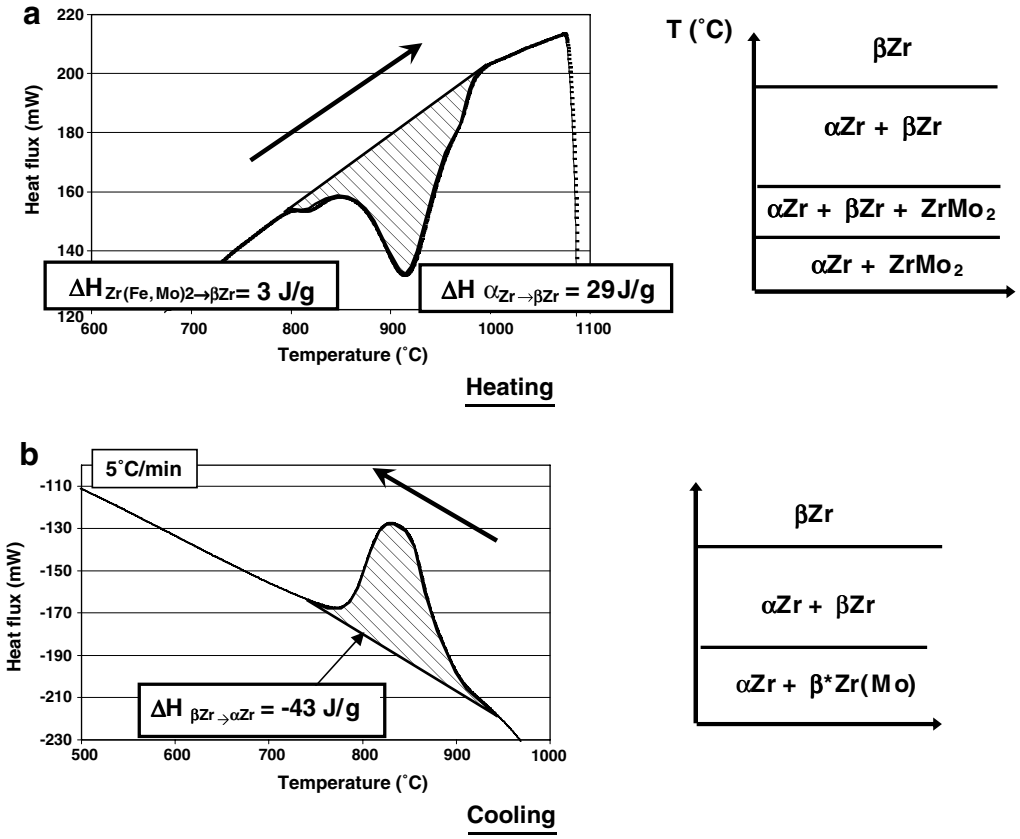

Fig. 10. Typical thermogram obtained by calorimetry on Zr–1.2 wt%Sn–0.5 wt%Mo–0.03 wt%Fe.

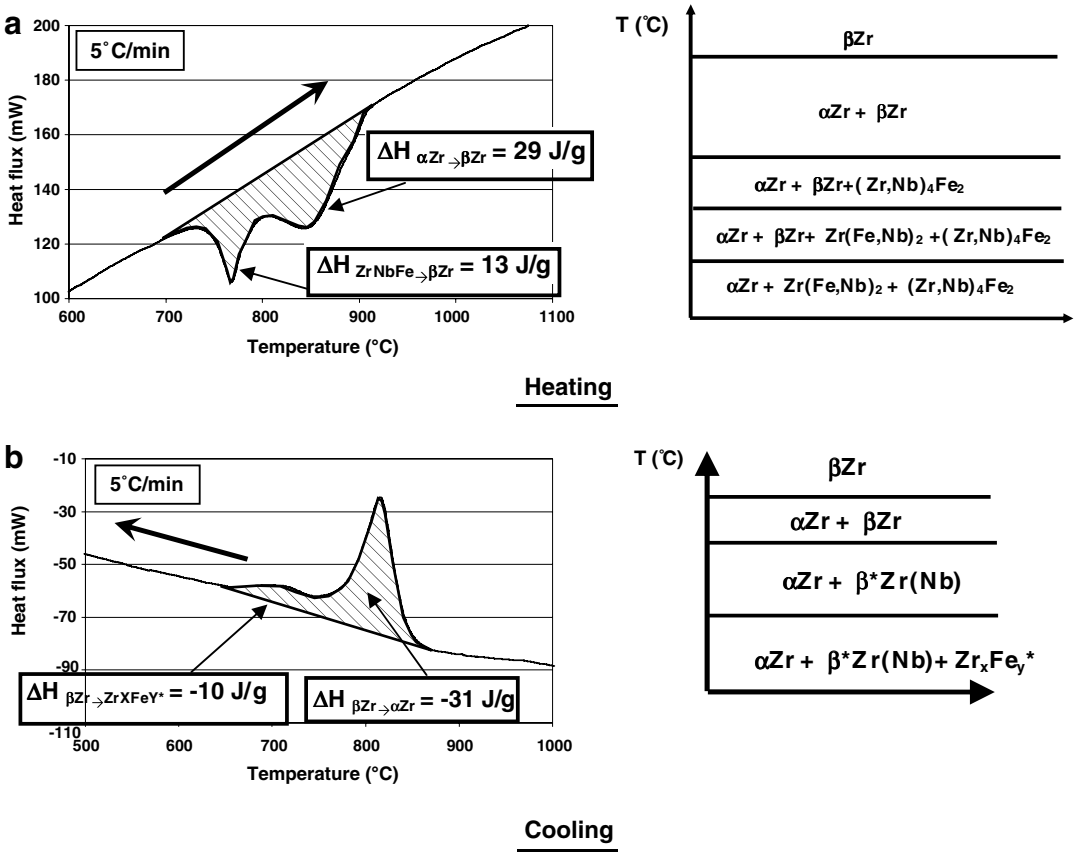

Fig. 11. Typical thermogram obtained by calorimetry on Zr–0.8 wt%Nb–0.5 wt%Fe.

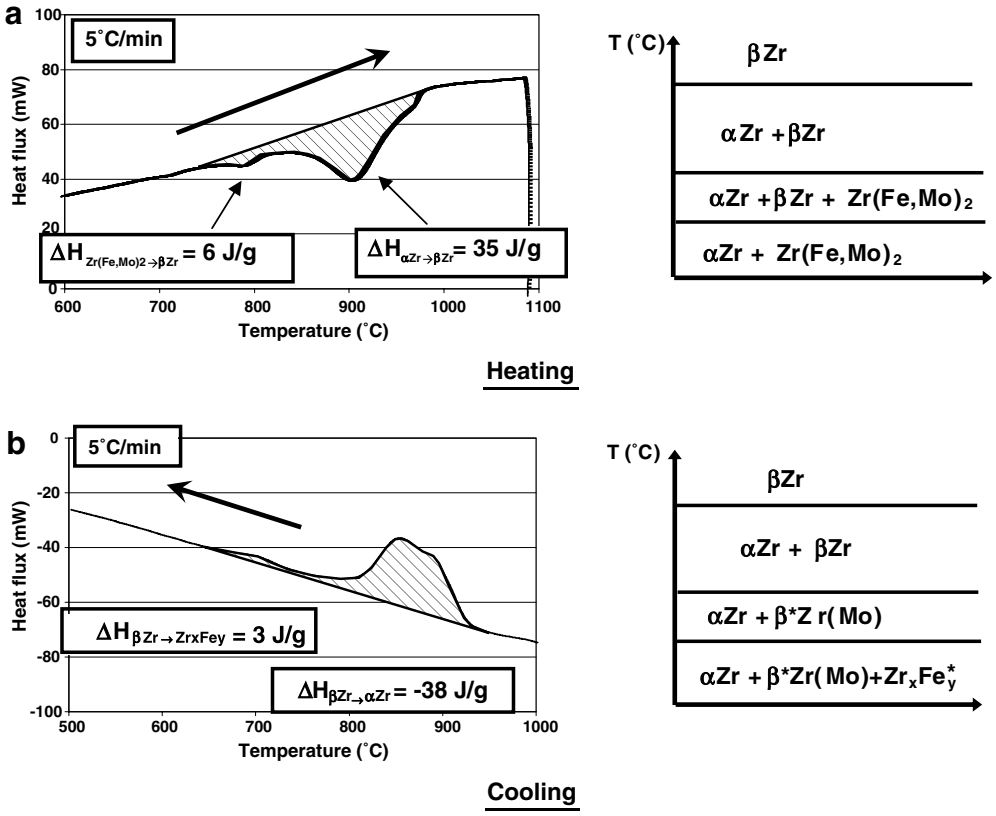

Fig. 12. Typical thermogram obtained by calorimetry on Zr–1.2 wt%Sn–0.2 wt%Mo–0.2 wt%Fe.

4.4.2.2. Zr–Sn–Mo, Fe. A similar behaviour is observed for the alloy: Zr–1.2 wt%Sn–0.2 wt%Mo–0.2 wt%Fe. The reaction upon heating and cooling is not reversible (Fig. 12). After one thermal cycle, two metastable phases can be retained at room temperature: $Zr_xFe_y^*$ and β_{Zr}^* phases (that is β_{Zr} enriched in Mo (~15 at.%Mo)).

5. Discussion

5.1. SPP's types and metastability as a function of the alloy family

From the above results, calorimetry appears to be a powerful tool in order to follow the phase transformations progress upon heating/cooling, even for low volumic fractions of SPPs. However, these determinations need some complementary direct microstructural investigations (TEM and/or neutron diffraction) to identify clearly the different types of SPPs.

The different alloys studied in this work can be separated into two groups of alloys. The first group consisting of Zircaloy type and Zr–Sn(Fe, V) alloys, is characterized by reversible transformation reactions upon heating and cooling. On heating, the allotropic $\alpha_{Zr} \rightarrow \beta_{Zr}$ transformation reaction starts around 800 °C. The transformation of SPPs also takes place around 800 °C and is assumed to be an 'inverse eutectoid' type reaction: SPP + $\alpha_{Zr} \rightarrow \beta_{Zr}$.

Table 3
Typical data concerning SPPs phase transformations

Alloys type	Zr–Sn(Fe, Cr)	Zr–Sn(Fe, V)	Zr–Nb–Fe(Sn)	Zr–Sn–Mo, Fe
SPPs type	$Zr(Fe,Cr)_2$	$Zr(Fe,V)_2$	$Zr(Nb,Fe)_2(Zr,Nb)_4Fe_2\beta Nb$	$Zr(Fe,Mo)_2$
Transformation/ precipitation temperature of SPPs (in °C)	~800	~780–850	~600–760	~700–750
Typical diffusion distance ($2\sqrt{Dt}$) in β_{Zr} after 5 min at the precipitation temperature	$\lambda_{Fe} \sim 60$ μm $D_{(Fe-800\,°C)} = 2.8E^{-12}$ m^2 s^{-1} [23] $\lambda_{Cr} \sim 10$ μm $D_{(Cr-800\,°C)} = 1.2E^{-13}$ m^2 s^{-1} [23]	$\lambda_{Fe} \sim 60$ μm $D_{(Fe-815\,°C)} = 3.4E^{-12}$ m^2 s^{-1} [23] $\lambda_{V} \sim 1$ μm $D_{(V-815\,°C)} = 4.6E^{-16}$ m^2 s^{-1} [24]	$\lambda_{Fe} \sim 25$ μm $D_{(Fe-680\,°C)} = 5.8E^{-13}$ m^2 s^{-1} [23] $\lambda_{Nb} \leqslant 1$ μm $D_{(Nb-680\,°C)} = 7.2E^{-16}$ m^2 s^{-1} [25]	$\lambda_{Fe} \sim 35$μm $D_{(Fe-680\,°C)} = 1.1E^{-12}$ m^2 s^{-1} [23] $\lambda_{Mo} \leqslant 1$ μm $D_{(Mo-725\,°C)} = 6.7E^{-16}$ m^2 s^{-1} [23]

The second group of alloys corresponds to Zr–Sn–Mo, Fe and Zr–Nb–Fe(Sn) alloys. The transformation reactions of these alloys are not reversible upon heating and cooling even for slow heating/cooling rates. Non reversibility of the transformation reaction has been previously confirmed by in-situ Neutron diffraction experiments on two ZrNbFe alloys: Zr–1 wt%Nb–0.75 wt%Fe and Zr–2 wt%Nb–0.45 wt%Fe [20]. In these alloys, the equilibrium SPPs present at low temperatures are respectively a FCC $(Zr, Nb)_4Fe_2$ phase ($a = 12.1$ Å) and/or a HCP $Zr(Nb, Fe)_2$ phase ($a = 5.5$ Å and $c = 8.7$ Å). After transforming these

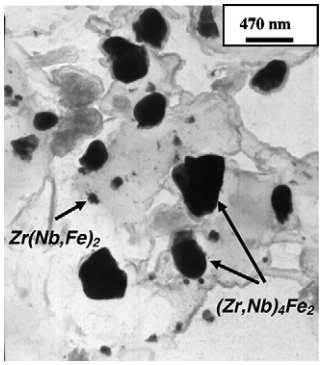

Fig. 13. TEM micrograph of a carbon replica obtained on a Zr–0.5 wt%Nb–0.5 wt%Fe annealed 1000 h at 550 °C (before the calorimetric cycle).

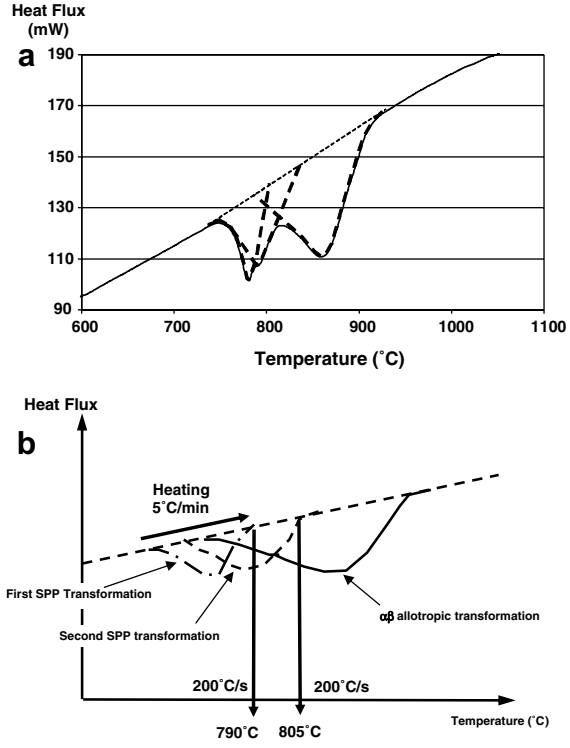

Fig. 14. Alloy Zr–0.5 wt%Nb–0.5 wt%Fe: Portion of thermogram obtained upon heating (the dotted lines materialize the different peaks) and schematic representation of the thermal treatment applied in order to determine which SPP transforms at first.

Table 4
Alloy Zr–0.5%Nb–0.5%Fe: phase precipitated after heating at 5 °C/min and cooling at 200 °C/s from 790 and 805 °C, as observed by TEM on carbon replica

SPPs type after quenching from 790 °C	SPPs type after quenching from 805 °C
$(Zr, Nb)_4Fe_2$	Zr_3Fe^*
Zr_3Fe^*	
β^*_{Zr}	β^*_{Zr}

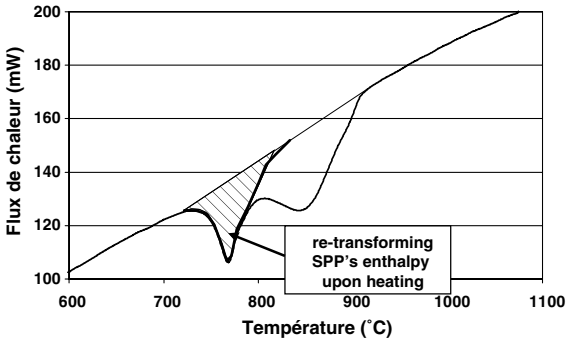

Fig. 15. Typical thermogram obtained upon heating showing deconvolution of the endothermic peak corresponding to the re-transformation of the SPPs.

SPPs into β_{Zr} phases upon heating, it is shown that metastable $Zr_xFe^*_y$ and β^*_{Zr} phases can precipitate upon cooling.

For Zr–Sn–Mo, Fe alloys, we have observed that 24 h annealing at 700 °C was not enough in order to fully transform the metastable β^*_{Zr} phase (enriched in Mo) into equilibrium intermetallic phases ($ZrMo_2$ or $Zr(Fe, Mo)_2$). The slow transformation kinetics of metastable $\beta^*_{Zr(Mo)}$ phase has been confirmed by different authors: among Domagala et al. [21], the isothermal transformation $\beta \rightarrow \alpha + ZrMo_2$ is achieved after 24 h at 700 °C for an alloy containing 1.3 wt%Mo and after 1 week for an alloy containing 5.4 wt%Mo. Zakharova and Vasil'eva have also studied the transformation kinetics of metastable β^*_{Zr} phases in two different alloys Zr–14 wt%Nb–12 wt%Mo and Zr–24 wt%Nb–9 wt%Mo at three temperatures: 350, 550 and 750 °C [22].

For a Zr–1 wt%Nb alloy, we have already shown that it was necessary to anneal up to 2000 h at 570 °C in order to fully transform the metastable β^*_{Zr} (enriched in Nb) into equilibrium the $\alpha_{Zr} + \beta_{Nb}$ phases [6]. Thus, for this group of alloys, the determination of SPPs fractions and existence temperature ranges by calorimetry has to be limited to the first heating. Furthermore, in a previous study [20], we pointed out the necessity to perform a long-term pre-annealing treatment in the α temperature range in order to obtain the quasi-equilibrium phase fractions.

The reversibility and non-reversibility of the transformation reactions can be simply estimated by calculating the diffusion distance in the matrix ($2\sqrt{Dt}$ where D is the diffusion coefficient and t is the time) of the different alloying elements at the typical precipitation temperatures (after

Table 5
Pre-annealed Zr–Nb–Fe(Sn) alloys: Calculated SPP's fractions and associated re-transformation ($\Delta H_{SPP \rightarrow \beta Zr}$) enthalpy deduced from calorimetric thermograms

Alloys composition	Pre-annealing treatment (in h/°C)	Calculated atomic fraction of SPP's (including β_{Nb}) (%)	$\Delta H_{SPP \rightarrow \beta Zr}$ upon heating at 5 °C/min (J/g)
Zr–0.55%Nb	5000/570	0.15	1.5
Zr–1%Nb	5000/570	0.6	4
Zr–2.5%Nb	5000/570	2.2	12
Zr–1Nb–0.75Fe	1800/570	3.3	11
Zr–2Nb–0.45Fe	1800/570	3.5	15
Zr–2Nb–0.75Fe	1800/570	4.61	18
Zr–1.1Nb–0.5Sn–0.4Fe	1800/570	2.45	12
Zr–0.4Nb–0.5Fe	1000h/500	2	10
Zr–0.5Nb–0.5Fe	1000/500	2.2	12
Zr–0.85Nb–0.5Fe	1000/500	2.5	12

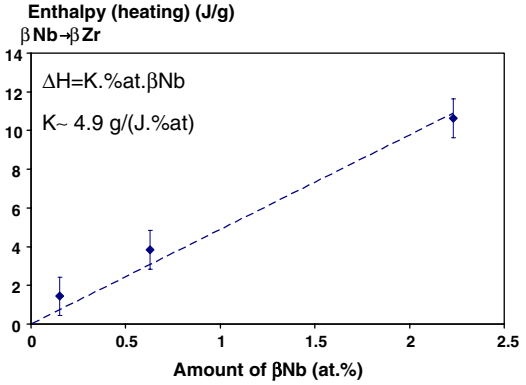

Fig. 16. βNb phases: correlation between amount of phases and re-transformation enthalpies determined by calorimetry upon heating at 5 °C/min.

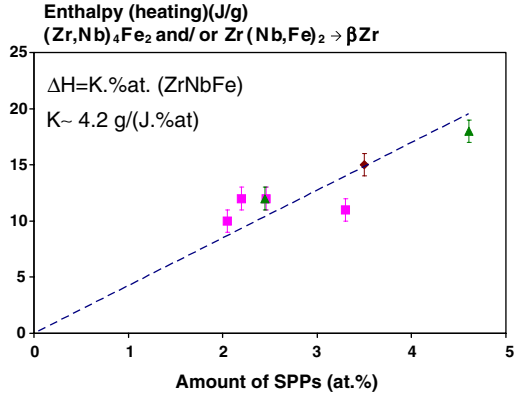

Fig. 17. ZrNbFe SPPs: correlation between amount of phases and transformation enthalpies determined by calorimetry upon heating at 5 °C/min.

5 min). Typical values are reported in Table 3. It clearly appears that Nb and Mo are much slower diffusing atoms than the Fe, Cr and V ones.

Moreover, the typical diffusion distance of Nb and Mo in β_{Zr} at the typical SPP's precipitation temperatures appear to be too small to allow the full precipitation of equilibrium SPP's upon cooling, even at low cooling rates.

5.2. Particular case: Successive SPP's re-transformations upon heating

In some cases, two intermetallic SPPs were initially precipitated and this was illustrated by the existence of two endothermic peaks upon heating on the associated thermograms. In order to determine which phase was the first one to be transformed upon heating, we performed heatings at 5 °C/min up to different temperatures and then a quenching at 200 °C/s from these temperatures to room temperature. This is illustrated here on the alloy Zr–0.5 wt%Nb–0.5 wt%Fe. The equilibrium SPPs precipitating at low temperatures are: $Zr(Nb,Fe)_2$ and $(Zr,Nb)_4Fe_2$ (see Fig. 13). Two convoluted peaks corresponding to the SPPs phase transformation were then detected by calorimetry upon heating. The initial and final transformation temperatures of the SPPs were deduced from the thermograms. Two heatings were performed: one stopped at a temperature corresponding to the end of the first peak (i.e., ~790 °C) and the other one at the end of the second peak (i.e., ~805 °C) as illustrated in Fig. 14.

The resulting microstructures have then been characterized by TEM-EDS analysis on carbon extractive replica. The results are presented in Table 4. The resulting microstructure after cooling from 790 °C is constituted by metastable Zr_3Fe^* and Nb enriched β^*_{Zr} and $(Zr,Nb)_4Fe_2$ SPPs. This shows that $(Zr,Nb)Fe_2$ is the first SPP that re-transforms upon heating.

This also shows that the calorimeter is sensitive enough to detect the successive on-heating re-transformation of two SPPs with a low volumic fraction ($\leqslant$1%).

5.3. Correlation between the SPP's fractions and the measured calorimetric enthalpy upon heating

The SPPs volume fractions have been calculated taking into account the alloys' nominal composition, the chemical compositions of the phases, the solubility limit of Nb in α_{Zr}

Table 6
Typical data concerning α_{Zr}/β_{Zr} allotropic phase transformation compared to the SPP's transformation/precipitation temperatures

Groups	*Group 1*: Zr–Sn(Fe, Cr, V) Zircaloy type alloys		*Group 2*: Zr–Mo, Nb–(Fe, Cr, Sn) alloys	
Alloys type	Zr–Sn(Fe, Cr)	Zr–Sn(Fe, V)	Zr–Nb–Fe(Sn)	Zr–Sn–Mo, Fe
$T_{\alpha/\alpha+\beta}$	~810–825 °C	~780–800 °C	~600 °C	~725 °C
Phase β^*_{Zr} retained at 20 °C	No	No	Yes (%Nb ~ 15–20%)	Yes (%Mo ~ 15%)
Isothermal transformation kinetic of β^*_{Zr}	–	–	Slow ≈ 2000 h at 570 °C	Slow > 24 h at 700 °C
SPPs	$Zr(Fe, Cr)_2$	$Zr(Fe, V)_2$	$Zr(Nb, Fe)_2$,$(Zr, Nb)_4Fe_2$,β_{Nb}	$Zr(Fe, Mo)_2$
Transformation/precipitation temperature of SPPs	~800 °C	~780–850 °C	~600–760 °C	~700–750 °C

and assuming that all the available amount of Fe had precipitated. This strong assumption is consistent with the fact that the equilibrium solubility limit of Fe in α_{Zr} at low temperatures is known to be less than ~100 wt ppm [23]. For instance, for an alloy containing $\alpha_{Zr} + Zr(Nb,Fe)_2 + \beta_{Nb}$ phases, this leads to the following equations:

$$f_1\,[Nb]_{\alpha Zr} + f_2\,[Nb]_{Zr(Nb,Fe)2} + f_3\,[Nb]_{\beta Nb} = [Nb]_{alloy}$$
$$f_1\,[Fe]_{\alpha Zr} + f_2\,[Fe]_{Zr(Nb,Fe)2} + f_3\,[Fe]_{\beta Nb} = [Fe]_{alloy}$$
$$f_1 + f_2 + f_3 = 1$$

where:

f_1: α_{Zr} molar fraction
f_2: $Zr(Nb, Fe)_2$ molar fraction
f_3: β_{Nb} molar fraction
$[Nb]_{\alpha Zr}$: Nb concentration in α_{Zr} (solubility limit)
$[Nb]_{Zr(Nb, Fe)2}$: Nb concentration in $Zr(Nb, Fe)_2$
$[Fe]_{Zr(Nb,Fe)2}$: precipitated Fe fraction
$[Nb]_{alloy}$: Nb nominal concentration in the alloy
$[Fe]_{alloy}$: Fe nominal concentration in the alloy
$[Nb]_{\beta Nb}$: Nb concentration in β_{Nb} (~80–90 at.%)
$[Fe]_{\alpha Zr} \sim 0$ and $[Fe]_{\beta Nb} \sim 0$

Pre-annealed Zr–Nb–Fe(Sn) alloys have been studied by calorimetry. Long-term enough pre-annealing treatments at low temperature (<600 °C) were performed in order to guarantee a full precipitation of the SPPs (in order to achieve quasi-equilibrium fractions).

The enthalpies were determined from the calorimetric thermograms assuming gaussian peaks (for deconvolution) as illustrated in Fig. 15.

The values of the enthalpies determined from calorimetric measurements are reported in Table 5.

Figs. 16 and 17 represent the correlation between the amount of initial SPP's and the re-transformation enthalpy determined by calorimetry upon heating at 5 °C/min for the different alloys studied.

Taking into account the various nominal chemical compositions of the alloys studied and the uncertainty of the measurements, the calorimetric determinations show a quite good correlation with the total amount of SPP's. High sensitivity-high temperature calorimetry appears to be a useful facility to estimate the fraction of SPP's and the re-transformation temperature ranges upon heating.

6. Conclusion

This work allowed to demonstrate that high temperature DSC is sensitive enough to detect phase transformations of SPPs even for small volume fractions (~1%) as a function of temperature in low alloyed Zr alloys.

Different kinds of alloys were studied: they can be separated into two groups as summarized in Table 6.

Group 1: Zr–Sn(Fe, Cr, V) Zircaloy type alloys.
Group 2: Zr–Mo, Nb–(Fe, Cr, Sn) alloys.
These two groups are mainly characterized by:

(a) Allotropic phase transformation α_{Zr}/β_{Zr}:
Group 1: this reaction is reversible, with low hysteresis (⩽50 °C)
Group 2: this transformation is not fully reversible, and the hysteresis is higher.
(b) Re-transformation/precipitation of the SPPs:For group 1, the transformation/precipitation of SPPs takes place at ~780–850 °C.
It takes place at lower temperatures for the alloys of group 2: 600–760 °C for Zr–Nb–Fe(Sn) alloys and 700–750 °C for Zr–Sn–Mo, Fe alloys, respectively. For these 2 last alloys, due to the low diffusivity of Nb and Mo, it is thus necessary to perform long-term enough annealing treatments to obtain quasi-equilibrium SPP's precipitated fractions in the α_{Zr} low temperature range.

Acknowledgements

Authors thank P. Olier and Ph. Parmentier from CEA-DRT-LTMEX and J.P. Mardon, P. Barberis from AREVA-NP for supplying some of the experimental alloys.

References

[1] F. Garzarolli, R. Holzer, J. Br. Nucl. Soc. 31 (1992) 65.
[2] P. Barberis, E. Ahlberg, N. Simic, D. Charquet, C. Lemaignan, G. Wikmark, et al., Role of the Second-Phase Particles in Zirconium

Binary Alloys, in: 13th Int. Symp. Zirconium in the Nuclear IndustryASTM STP, vol. 1423, ASTM International, West Conshohocken, PA, 2002, p. 33.
[3] D. Charquet, E. Alheritiere, Workshop on Second-Phase Particles in Zircaloy, F.R.G. Kerntechnische Gessellschaft, 1985, p. 5.
[4] A.T. Motta, K.T. Erwin, O. Delaire, R.C. Birtcher, Y. Chu, J. Maser, D.C. Mancini, B. Lai, in: Proc. of Thirteenth Int. Symp. ASTM STP 1423 of Zirconium in the Nuclear Industry, 2002, p. 59.
[5] Y.T. Zhu, J.H. Devletian, Determination of Equilibrium Solid-Phase Transition Temperature Using DTA, Metallurgical Transactions A 22A (September 1991) 1993–1998.
[6] C. Toffolon, J.C. Brachet, T. Guilbert, D. Hamon, S. Urvoy, C. Servant, D. Charquet, L. Legras, J.P. Mardon, J. Phys. IV France 11, 2001, p. 1.
[7] P. Van Effenterre, G. Cizeron, P. Lacombe, J. Nucl. Mater. 31 (1969) 269.
[8] T. Forgeron, J.C. Brachet, F. Barcelo, A. Castaing, J. Hivroz, J.P. Mardon, C. Bernaudat, in: Proc. of Twelfth Symposium on Zirconium in the Nuclear Industry, ASTM STP 1354, 2000, p. 256.
[9] C. Toffolon-Masclet, J.C. Brachet, G. Jago, J. Nucl. Mater. 305 (2003) 224.
[10] B. Vandersande, A.L. Bement, J. Nucl. Mater. 52 (1974) 115.
[11] V.V. Petkov, V.N. Svechnikov, Dopovidi Akademi Nauk Ukrains'koi Rsr, Seriya A: Fiziko-teknichni ta matematichni nauki 32 (7) (1972) 664.
[12] H. Fujii, T. Okamoto, W.E. Wallace, F. Pourarian, T. Morisaki, J. Magn. Magn. Mater. 46 (1985) 245.
[13] V.V. Petkov, A.V. Kotsyuruba, Seriya A: Fiziko-teknichni ta matematichni nauki 32 (8) (1972) 750.
[14] P. Rogl, H. Nowotny, F. Benesovsky, Monatshefte fuer chemie 104 (1973) 104.
[15] J.N. Yelim, O.T. Woo, G.J.C. Carpenter, J. Electron Microsc. Tech. 15 (1990) 400.
[16] A.V. Nikulina, V.N. Shishov, M.M. Peregud, A.V. Tselischev, V.K. Shamardin, G.P. Kobyliansky, J. Nucl. Mater. 238 (1996) 205.
[17] V.V. Petkov, E.E. Cherkashin, Dopovidi Akademi Nauk Ukrains'koi Rsr, Seriya A, Fiziko-teknichni ta matematichni nauki 32 (3) (1972) 276.
[18] Z.M. Alekseeva, N.V. Korotkova, Izvestiya Akademii Nauk. SSSR. Metally 1 (1989) 199.
[19] N.V. Korotkova, Z.M. Alekseeva, Izvestiya Akademii Nauk. SSSR. Metally 3 (1989) 207.
[20] C. Toffolon-Masclet, J.C. Brachet, C. Servant, L. Legras, D. Charquet, P. Barberis, J.P. Mardon, in: Proc. of Thirteenth International Symposium on Zirconium in the Nuclear Industry, June 10–14 2001, Annecy, France, ASTM STP 1423, 2002, p. 361.
[21] R.F. Domagala, D.W. Lewinson, D.J. Mc Pherson, Trans. AIME 209 (1957) 1191.
[22] M.I. Zakharova, V.B. Vasil'eva, Phys. Met. Metall. 55 (33) (1983) 188.
[23] L.V. Pavlinov, Fiz. Met. Metalloved 24 (1967) 272;
L.V. Pavlinov, Phys. Met. Metallogr. (English Transl.) 24 (2) (1967) 70.
[24] R.P. Agarwala, S.P. Murarka, M.S. Anand, Acta Metall. 16 (1968) 61.
[25] G.P. Tiwari, M.C. Saxena, R.V. Patil, Trans. Indian Inst. Met. 26 (1973) 55.